

Ageing and cyclic behaviour of axially loaded piles driven in chalk

Buckley, R.M.¹, roisin.buckley13@imperial.ac.uk

Jardine, R.J.¹,

Kontoe, S.¹,

Parker, D.¹,

Schroeder, F.C.²

1. Department of Civil & Environmental Engineering, Imperial College London, UK 2. Geotechnical Consulting Group LLP, London, UK

ABSTRACT

This paper reports a programme of static and cyclic loading tests on seven open steel tubes driven in low to medium density chalk at a well characterised test site, describing their response to driving, ageing *in situ* and loading under both static and cyclic conditions. Back analysis of dynamic monitoring identifies the distributions of notably low shaft resistances that develop during installation, showing that these depend strongly on the relative pile tip depth (h/R). The shaft capacities available to ‘virgin’ piles are shown to increase markedly after driving, following a hyperbolic trend that led to a fivefold gain after 250 days. Pre-failed piles do not follow the same trend when re-tested. Pile exhumation confirmed that driving remoulded the chalk, creating a puttyfied zone around the shaft. Excess pore water pressure dissipation, which is likely to have been rapid during and after driving, led to markedly lower water contents close to the shaft. Axial cyclic testing conducted around 250 days after driving led to a range of responses, from manifesting stable behaviour over 1000 cycles to failing after low numbers of cycles after developing sharp losses of static capacity. The dependence of permanent displacement on the cyclic loading parameters is explored and characterised. The experiments provide the first systematic study of which the Authors are aware into the effects of undisturbed ageing and cyclic loading on previously unfailed piles driven in chalk. Potential predictive tools may now be tested against the reported field measurements.

Keywords: chalk, cyclic loading, offshore engineering, piles, time dependence

(Main text around 5880 words)

INTRODUCTION

Open steel piles are driven routinely for port, bridge and offshore energy projects, including large numbers of offshore wind-turbines; Doherty *et al.* (2011). However, their design and installation is difficult when chalk is encountered. Chalk, a highly variable soft biomicrite composed of mainly silt sized crushable CaCO_3 particles, is found widespread across Northern Europe and under the North Sea, where thicknesses can exceed 1200m; Clayton *et al.* (2002), Mortimore (2012). While few carefully stage-loaded static load tests have been reported to prove or predict the piles' ability to carry axial loads, low shaft driving resistances (between 0 and 20kPa) have been reported from dynamic driving analyses that suggest low static service capacities (Lord *et al.*, 2002, Vijayvergiya *et al.*, 1977). The Construction Industry Research and Information Association (CIRIA) offers design guidelines based on four pile tests that indicate widely different ultimate unit shaft resistances of 20 to 120kPa for low-medium and high density chalks respectively (Lord *et al.*, 2002). These values appear remarkably low, given the intact chalk's Unconfined Compressive Strength (UCS) range of 1.25 to >12.5MPa (Bowden *et al.*, 2002) and cone tip resistances, q_c of 4 to > 50MPa (Power, 1982). The low static shaft capacities recommended by Lord *et al.* (2002) imply low shaft radial effective stresses even after full equalisation. Similar conclusions followed from Burland and French's (1990) tests on steel box piles, that could be expanded mechanically after driving. Their shaft friction capacities increased by almost 400% when the cross sectional areas were expanded by 14.3% following driving in low-medium density chalk. Stark choices have to be made when selecting design parameters that can impact significantly in projects involving potentially hundreds of large piles; Carrington *et al.* (2011).

Dynamic percussion damage during driving provides one explanation for low driving resistance. De-structuration and crushing of hollow calcium carbonate (CaCO_3) particles beneath the advancing pile tips produces low strength putty that spreads along the pile and limits drastically the radial effective stresses and shear resistances that can act on the shaft; Hobbs and Atkinson (1993), Lord *et al.* (2002). The shaft shear stresses available at any depth appear to attenuate with increasing relative distance from the pile tip, h , as the pile penetrates; Norrie (2015). Similar dependencies on " h/R " (where R is the pile radius) have been reported for clays and sands by Bond and Jardine (1991), Lehane and Jardine (1992a, 1992b), Lehane *et al.* (1993), Chow (1997) and Jardine *et al.* (2005a). Such trends were termed "friction fatigue" in clay by Heerema (1978) and for sand by Randolph *et*

al. (1994) and White (2005). High-level laboratory simple shear cyclic loading and cyclic cone penetration tests (CPT) have also been found to reduce the shear stresses that intact chalk can carry to as low as 4kPa (Carrington *et al.*, 2011, Diambra *et al.*, 2014). However, large diameter offshore piles have been known to free-fall considerable distances rapidly in chalk without any hammering (Norrie, 2015); dynamic load cycling is not essential to low installation resistances.

Dynamic monitoring often shows capacity growth over driving pauses. Long term beneficial time effects on static shaft resistance have been reported in sands (see Jardine *et al.* (2006), Rimoy *et al.* (2015) or Gavin *et al.* (2015)) and clays, e.g. Karlsrud *et al.* (2014). While Lord *et al.* (2002) suggested that field set-up (or increase in capacity with time) also takes place with low-medium density chalk, due to pore pressure dissipation and/or internal re-cementing of the putty annulus around the pile, redox chemical reactions may also play a role. Vijayvergiya *et al.* (1977) reported an 80% increase in dynamic driving resistance over a 60 day pause in an offshore project, while Skov and Denver (1988) interpreted a 383% increase over 13 days from static and dynamic load tests on two concrete piles driven in chalk. Lahrs and Kallias (2013) reported 50% to 60% increases in shaft resistance in chalk over four months from multiple offshore dynamic restrikes on 1.5m diameter piles, but found the shaft capacity of a single pile fell over time when subjected to multiple restrikes and a static test. Re-testing pre-failed piles is often misleading; pre-failed piles often show far less set-up than equivalent “virgin” piles in sands and clays; Jardine *et al.* (2006), Jardine and Standing (2012), Karlsrud *et al.* (2014). Ciavaglia *et al.* (2017b) described the results of three tension tests conducted on the same 0.762m diameter 4m long steel piles which showed shaft resistances increasing by up to 700% in re-tests conducted over four months. Their strain gauge readings indicated four to six times higher shaft resistances applying on the lower halves of the piles, as well as a significant deleterious effect of previous lateral loading.

Foundations are often subjected to repeated or cyclic loading under a wide range of loading rates. Offshore piles sustain wind and wave loading cycles during storms, while wind-turbines impose millions of rotating blade cycles (Jardine *et al.*, 2012). The effects of relatively slow (non-dynamic) wave load cycling can be investigated in field tests. Burland and French (1990) report that the tension capacity of their steel pile had reduced by 60% after 20 slowly applied axial cycles. However, little other guidance appears to be available regarding this potentially important factor. A range of procedures exist to address non-dynamic axial cycling for piles driven in sands and clays. Jardine *et al.* (2012) and Andersen *et al.* (2013) set out approaches involving empirical global methods,

local (T-z) analyses based on soil element or instrumented pile tests and fully implicit numerical techniques based on advanced constitutive models. Whilst the latter provide potentially the most powerful tools, difficulties arise in full implementation, see for example Buckley (2014). There is a clear need for reliable cyclic pile tests at chalk sites, supported by high quality site characterisation, to provide benchmarks against which potential predictive procedures may be developed, assessed and calibrated.

The above design guidance shortcomings pose significant risks for the potentially thousands of offshore wind-turbines planned for chalk sites. Barbosa *et al.* (2015) and Jardine (2017) outline a Joint Industry Project (JIP) research programme that aims to improve design reliability. This paper reports one element; field tests at St Nicholas at Wade, Kent, UK, on seven 139mm outside diameter steel tubular piles driven to 5.5m penetrations in low-medium density chalk. These experiments investigated:

- a) Dynamic resistances during driving;
- b) How pile installation and testing affected the chalk surrounding the pile shaft;
- c) Capacity-ageing trends for virgin piles over 8 months after installation;
- d) The impact of pre-testing to failure; and
- e) How multiple ‘virgin’ piles respond to large numbers of one-way non-dynamic axial load cycles after 8 months of ageing after driving.

PILE TESTS AT ST. NICHOLAS AT WADE

GROUND CONDITIONS

Recent and previous investigations

The experiments were conducted in a quarry close to St. Nicholas at Wade, 15km west of Margate, Kent where all overburden and weathered material has been removed to expose chalk from the Margate White Chalk subgroup which comprises 98.6% CaCO₃ (Hancock, 1975). Five boreholes were advanced to a maximum 20.5m depth and eleven CPTs to a depth of 17m in earlier site investigation studies (Setech, 2007, Fugro, 2012). Joint Industry programmes of static and slow (non-dynamic) cyclic lateral pile tests have been conducted along with axial testing on the same piles (Dührkop *et al.*, 2015, Ciavaglia *et al.*, 2017a, 2017b). Laboratory index, CRS

oedometer, UCS, static and cyclic direct simple shear and triaxial and resonant column tests have been performed in conjunction with cross-hole and down-hole seismic logging and pressuremeter tests. The Imperial College (IC) research tests were conducted on flat ground approximately 60m away from the previous study areas; see Fig. 1. New CPT tests with pore pressure measurement (CPTu) were undertaken in this area. Summaries of the profile, CPT traces and remarkably high piezocone u_2 pore pressures encountered are given in Fig. 2.

Laboratory testing

Classification tests, summarised in Table 1, show mainly low density chalk with intact dry densities (IDD) from 1.38 to 1.54Mg/m³ (Bowden *et al.*, 2002) with a medium density layer between 2.9 and 3.3m, where IDD reaches 1.64Mg/m³. While ground water is reported around 11.6m below the quarry base, the degree of saturation is high above the water table (Table 1). Bishop apparatus ring shear tests by the Authors against mild steel interfaces representing ‘field pile’ roughnesses, gave residual interface friction angles, δ_r between 30 and 31°; similar values were reported by Le *et al.* (2014) and Ziogos *et al.* (2016). Intact chalk is markedly brittle, failing at less than 0.1% local axial strain in triaxial tests (Jardine *et al.*, 1984). Lord *et al.* (2002) indicate intact c' values from 100kPa to > 2 MPa, with $36^\circ < \varphi' < 42^\circ$. Remoulded chalk generally mobilises φ' between 29 and 34° with $0 < c' < 10\text{kPa}$ (Clayton, 1978, Razoaki, 2000, Bundy, 2013). Peak failure stresses from triaxial tests on intact and remoulded samples from the site are shown on Fig. 3. Consolidated drained triaxial tests on *intact* samples show a markedly brittle response with best fit peak $c' = 390\text{kPa}$ and $\varphi' = 41^\circ$ developing at small strains (<0.2%) , while undrained triaxial compression tests on remoulded samples showed ductile behaviour with tentative peak φ' angles of between ≈ 36 and 38° (for low and medium densities respectively), when zero c' is assumed. Further details on the triaxial test results are included in Appendix A.

Cone penetration tests

Multiple CPT tests in the test area indicated q_c varying moderately spatially, showing the trend summarised in Fig. 4. Most q_c values fell between 10 and 20MPa, with a $100 < f_s < 500\text{kPa}$ range. Thin, discrete and discontinuous flint bands gave sharp local peaks in cone resistance up to 60MPa that are not thought to have influenced the pile tests unduly. The maximum pore pressures recorded exceeded 4MPa over the depth of interest. CPTu dissipation tests at 3.5 and 3.6m depth indicated 50% equalisation times, t_{50} of between 4 and

13 seconds, confirming findings by Diambra *et al.* (2014) and indicating radial coefficients of consolidation, c_h of 5 to 15 $\times 10^{-4}$ m²/year when suitable (high) rigidity indices are assumed for the intact chalk. The degree to which drainage takes place around the tips of piezocones or piles during steady penetration may be assessed from the non-dimensional velocity defined by Finnies and Randolph (1994) as:

$$V = \frac{vD}{c_h} \quad \text{Eq. 1}$$

Where D is the penetrometer diameter and v is its velocity. For CPTu pore pressure dissipation tests, the appropriate “operational” coefficient of consolidation, $c_{h, \text{piezo}}$ for use in Eq. 1 lies within the range $c_{h, \text{NC}} < c_{h, \text{piezo}} < c_{h, \text{OC}}$ where $c_{h, \text{NC}}$ and $c_{h, \text{OC}}$ are the values for normally consolidated and overconsolidated conditions, respectively (Leroueil *et al.*, 1995, Fahey and Lee Goh, 1995). Centrifuge tests on normally consolidated clays and silts show a transition from partially drained to fully undrained conditions at non-dimensional velocities between 10 and 100 when a $c_{h, \text{NC}}$ value is used in Eq.1; Finnies and Randolph (1994), Randolph (2004), Cassidy (2012), Suzuki (2014). Fahey and Lee Goh (1995) suggest that $c_{h, \text{piezo}}$ is around 5 $c_{h, \text{NC}}$, making the transition V range 2 to 20 when $c_{h, \text{piezo}}$ is employed. Applying these estimates to the 43.8mm diameter piezocones advancing at 20mm/s, gives $0.54 < V < 1.76$, indicating some partial drainage can be expected during penetration. The same conclusion results from assuming the CPTu end bearing mechanism extends approximately two diameters below the cone tip and noting that the dissipation tests indicate $40 \pm 15\%$ pore pressure dissipation over the 3.6 seconds required to pass through the failure zone.

PILE AND DRIVING DETAILS

Seven 139mm diameter, tubular steel (API 5CT Grade L80/N80) piles (DP) with an average wall thickness, t_{wall} of 8.5mm were driven on 19th October 2015 to penetrations of ≈ 5.5 m using a 4T Junttan SHK100-4 hydraulic impact hammer, leaving 1m of pile above ground to facilitate testing. Fig. 5 shows the blow count profiles recorded over the 4 to 16 minutes required to drive each pile. Principally coring behaviour was observed; the internal soil columns of DP1, DP4 and DP5 stood between 0.26 and 0.82m above ground at the end of driving, but remained 0.18 to 0.43m below ground with the other four piles. Strain gauges and accelerometers were attached near the heads of DP1, DP4 and DP7 and dynamic driving data recorded with Pile Driving Analyser (PDA) software.

Lim and Lehane (2014) highlight the intrinsic limitations and uncertainties of inferring static capacity from dynamic driving monitoring including the effects of delays following driving. The Authors avoided the latter by pre-installing all sensors and monitoring uninterrupted continuous driving. As detailed in Appendix B, back analysis of the measured force and velocity signals was conducted using IMPACT (Randolph, 2008) which includes explicit modelling of both the internal and external shaft resistance. The best matches between measured and calculated force and force times pile impedance, Z were obtained by applying 85 – 90% of the resistance on the outer shaft, which is consistent with trends reported from instrumented piles (Chow, 1997). The average End of Driving (EoD) total shaft load was 39.3kN. Fig. 6 presents the final profiles of total (internal and external) shaft resistance against depth. The average end bearing at EoD, including the contribution from the internal shaft resistance, was 15.8MPa. The average EoD external shaft shear stresses of 15 to 17kPa, comparable to the 11 to 23kPa range reported at EoD for 762mm diameter 4m long open steel piles driven at the same site by Ciavaglia *et al.* (2017b), fall 15 to 25% below the CIRIA 20kPa recommendation for static shaft capacity in low-medium density chalk (Lord *et al.*, 2002). However, markedly higher local resistances are interpreted over the lowest 1 to 1.5m of the shaft from the signal matching, which tend towards the CPTu f_s value of ≈ 200 kPa and decayed sharply with additional distance, h above the tip. The variations, which do not correlate with chalk property changes with depth, confirm a strong influence of “ h/R ” on installation shaft resistance.

Substituting $c_{h, \text{piezo}}$ and the field penetration velocities into Eq. 1 indicates partially drained behaviour for the piles with $0.25 < V < 3.07$, if the piles are considered open-ended with effective radii R^* . Scaling up from the piezocone dissipation t_{50} times by the ratio of $(R^*/R_{\text{CPTu}})^2$ and applying the static driving velocity ranges of the piles, allows the h values at which tip generated pore pressures dissipated by 50% to be estimated as 210 to 690mm. Higher degrees of equalisation can be expected at greater h values, where longer times elapse after the local excess pore pressures were generated at the tip. The chalk putty annulus formed around the shaft is likely to experience degrees of consolidation and void ratio reduction during driving that depend on h/R . Given the kinematic restraint provided by the surrounding stiff chalk mass, the putty’s volume straining will also reduce the effective stresses acting on the pile shaft. Lower degrees of shaft ‘consolidation during driving’ are likely to apply to larger piles and/or those that penetrate more rapidly, as in the free falling ‘pile runs’ that can occur when installing large monopiles in chalk (Norrie 2015).

THE EFFECTS OF PILE INSTALLATION ON THE SURROUNDING CHALK MASS

Conditions surrounding the shaft of the aged piles were examined by partial exhumation of two piles after testing. Trial pits were excavated to maximum 1.1m depth adjacent to DP1 and DP7, 274 days after driving. A schematic description of the chalk fabric developed around the piles is shown on Fig. 7, while Fig. 8 shows the variations in water content with depth, z and normalised radial distance from the pile centre, r/R . The conditions observed around the piles can be summarised as:

- **Zone A:** 0-14mm from pile wall, remoulded chalk (assumed to have puttified during driving) with no distinct features. A 1-2mm thick mottled brown oxidised surface adjacent to the surface of the pile giving evidence of redox reactions involving the pile steel. Water contents (w_c) range from 19.5 to 24.9% (average = 22.8%), falling below the undisturbed far-field average of 29.9%;
- **Zone B:** 14-50mm from pile wall – intact chalk with gritty fragments, crumbles between fingers into dice sized blocks. Evidence of recent fracturing with no iron staining; w_c ranges from 25 to 28% (average = 26.5%). This zone is discontinuous and was not encountered at all depths;
- **Zone C:** Intact chalk which breaks into bigger blocks. Fractures iron stained (old) and open to <3mm; w_c ranges from range 26.4 and 31.3%, with the average of 28.4% slightly lower than the far-field mean.

The remoulded zone's thickness, t_{zone} varied from 0.59 to 1.64 times the pile wall thickness as shown on Fig. 7 and Fig. 8. Muir Wood *et al.* (2015) exhumed a previously tested 762mm diameter pile and report a remoulded annulus of 0.78 to 1.57 times t_{wall} . The same Authors found remoulded zones formed around steel driven plates whose width amounted to approximately 40% of the varying plate's thicknesses. Evidence of the conditions under which the remoulded zone formed was presented in the present study by natural fractures and marl seams which terminated and curved sharply downwards at the zone's outer edge. There was no sign of any shear surface close to the pile, or within the chalk mass, having formed during static loading, that could be separated confidently from the remoulded zone that formed during driving. As argued earlier, the remoulded zone probably underwent at least partial contemporaneous consolidation that contributed to the driving 'h/R' effects identified in Fig. 6 through relaxation of the shaft radial effective stresses. Jardine *et al.* (2006, 2013) argue that similar radial effective stress reductions take place around piles driven in sand and that subsequent

creep processes allow the arching mechanisms generated around the shafts to relax and so contribute to shaft capacity growth with time.

STATIC AND CYCLIC TESTING PROGRAMME

The dynamic driving analysis provided estimates for the piles' average EoD 'initial' compressive shaft resistance. The post-driving ageing trends were tracked by 'slow' static tension tests conducted at four ages on three virgin piles, and one pre-tested pile, as summarised in Table 2.

The effects of slow (non-dynamic) cyclic loading on aged piles were investigated through the separate programme summarised in Table 3, testing four virgin piles 247 to 255 days after driving. The first cyclic experiment, DP7, imposed 1000 medium level cycles before a 'quick' static test to failure in tension. Piles DP1, DP4 and DP5 were initially all subjected to ≥ 1000 relatively low level cycles, which led to little or no stiffness loss and modest displacements. Two of the three piles (DP1 and DP5) were then subjected, without delay, to cycling at higher normalised load levels. 'Quick' tension load tests to failure followed in both cases. Pile DP4 was initially subjected to 1000 relatively low level cycles, followed immediately by a "quick" static test to failure. A second higher level cyclic test was performed six days later.

EXPERIMENTAL PROCEDURES

The static and cyclic tests were all conducted with the load and control equipment shown in Fig. 9, which was designed and built at Imperial College. The static and cyclic tests were conducted in tension to allow the shaft friction to be determined without any base instrumentation, which was not feasible for the tests in this study. Pile head displacements were monitored by three Linear Variable Differential Transformers (LVDTs) spaced evenly circumferentially around the pile and attached to an independent reference frame supported on stands set 1m from the pile centre. The 'slow' static test loads were applied in increments of 10% of the expected failure capacity, each imposed over 1 minute, followed by monitored pause periods that extended as failure approached. Pile failure was defined as either i) displacement reaching 10% of the diameter, D or ii) the semi-logarithmic pile creep-displacement rate k_s measured under constant load exceeding 0.2mm/log cycle of time after ten or more minutes. The latter rate was scaled from the Ea-Pfähle (2014) criterion of $k_s > 2\text{mm per log cycle of time}$ to reflect the test pile dimensions. The load steps and creep pause durations depended on the creep monitoring data. Ten to twelve load steps were required to reach failure and tests took two to three hours

to complete. Additional ‘quick’ load tests were performed following selected cyclic tests that led to failure in less than thirty minutes.

The cyclic loading system could impose two to four cycles per minute (0.03 to 0.06 Hz) for thousands of cycles and control the peak loads to $\pm 2\%$. Sine wave loading was not achievable with the systems available. The adopted square wave, plus twin exponential section, cyclic load characteristic is shown in Fig. 10, where the average (Q_{mean}) and cyclic (Q_{cyc}) loading components are also defined. Table 5 lists the cyclic loading parameters associated with each test, which are referred to the *current* net static tension capacity, Q_t , of each pile, proven by the independent static test results. Cyclic failure manifests as rapidly accumulating permanent displacement and decreasing global stiffness and failure was defined as either i) permanent displacement reaching 0.1D (Yang *et al.*, 2016) or ii) a sudden increase in the rate of displacement accumulation, indicative of decreasing stability and approaching cyclic failure.

AGEING OBSERVATIONS

Tension tests were conducted to failure 10, 106 and 246 days after driving on three virgin piles; DP2, DP3 and DP6, which gave the peak capacities, corrected for pile and chalk plug self-weight, summarised in Table 4. Reverse end bearing is assumed negligible as the fractured chalk drains very rapidly and final static holding periods were typically greater than 30 minutes, far exceeding the dissipation time anticipated for any reverse end bearing mechanism. The piles' overall net axial load displacement responses are shown in Fig. 11, along with the average compressive EoD shaft capacity of DP1, DP4 and DP7 from the dynamic analysis described in Appendix B. Fig. 12 plots the peak static tension loads, corrected for pile and soil self-weight divided by the EoD compressive shaft capacity, against time. The closed symbols indicate the Intact Ageing Characteristic (IAC) of the virgin piles (Jardine *et al.* (2006)), while the open symbol shows the retest on pile DP2, completed 227 days after installation and 217 days after its 10 day static tension failure. If compression and tension shaft capacities are equal, then Fig. 12 indicates a set up factor of 5.2 after 246 days for the fresh piles, with mean shaft resistance growing from ≈ 16 to 86 kPa. Most of the beneficial ageing occurs over the first 100 days; the rates of change slow with time and may tend to a final equilibrium.

Empirical relationships have been suggested to represent such trends in clays and sands (Skov and Denver, 1988, Mesri *et al.*, 1990, Bogard and Matlock, 1990, Tan *et al.*, 2004). The hyperbolic relationship suggested by Tan *et al.* (2004) appears appropriate, where the shaft capacity Q available at time t is:

$$Q(t) = Q_u \left[m + (1 - m) \left(\frac{\frac{t}{T_{50}}}{1 + \frac{t}{T_{50}}} \right) \right] \quad \text{Eq. 2}$$

where Q_u is the projected ultimate equilibrium capacity, T_{50} is the time required to achieve 50% of Q_u and m is an empirical coefficient (around 0.2) applied to improve the fit at the early ($t < 1$ day) age. The curve plotted on Fig. 12 corresponds to $Q_u = 225\text{kN}$, $m = 0.2$ and $T_{50} = 27$ days. The single re-test confirmed that beneficial ageing was disrupted by previous static failure; the pre-failed DP2 showed 32% less gain in capacity over its 10 to 227 day age range than the equivalent virgin pile DP6.

The three static tests shown on Fig. 11 appear to follow similar initial global stiffness trends before curving towards their age-dependent failure loads. Global secant stiffness can be quantified as load change ΔQ from the initial 'nip-load,' applied to ensure loading system stability, divided by total displacement from the same origin.

The three tests' stiffness trends are plotted over the course of each stage in Fig. 13, along with the retest on pile DP2. The stiffness-load trends show highly non-linear trends from their first increment onwards, as is common in soils (Jardine *et al.*, 2005b). All three virgin curves share broadly similar initial stiffness of 100 to 200kN/mm at a 20kN load level, with the 106 and 246 day aged piles also showing similar stiffnesses over a range of loading levels. The re-tested pile shows significantly stiffer behaviour initially, which subsequently degraded at lower load levels than the virgin piles.

CYCLIC TEST RESULTS & INTERPRETATION

The definitions of the accumulated cyclic displacement parameters applied to the cyclic tests were given by Rimoy *et al.* (2013). The growth of permanent displacement, s_{acc} normalised by D , with the number of cycles, N , is plotted for the six cyclic experiments in Fig. 14 and 15. The four non-failing tests (Fig. 14 a to d) follow approximately constant logarithmic gradients once $N > 20$. The implied power law trends have the form:

$$\frac{s_{acc}}{D} = AN^B \quad \text{Eq. 3}$$

where A and B are non-dimensional fitting parameters. The re-test presented in Fig. 14 e) shows a broadly comparable but more staggered trend. The two unstable tests, presented in Fig. 15, failed at low N values and, as discussed later, demonstrated marked losses of shaft capacity.

The six tests' normalised Q_{mean} and Q_{cyc} loading components are plotted on an axial cyclic interaction diagram (Karlsrud *et al.*, 1986, Poulos, 1988, Jardine and Standing, 2000, 2012) on Fig. 16. In this Figure, the numbers of cycles imposed are also noted, falling below 1000 for the two tests that failed cyclically. The tension capacities employed to normalise the loads for each test age were obtained from Eq 2, as given in Table 5. The top-left to right-bottom diagonal in this diagram represents the static failure conditions, where the Utilisation of tension shaft capacity Ratio, $UR = Q_{max}/Q_t$ is equal to 1. The line representing the minimum $UR = 2/3$ recommended by API and ISO guidance for extreme offshore environmental loading cases is also shown, along with an $UR = 0.5$ line. Tentative contours of $N = 10$, 100 and 1000 are plotted to indicate the conditions under which cyclic failure could be expected under given normalised cyclic load combinations.

Axial cyclic stiffness

The experiments also revealed how global cyclic secant stiffness evolved during each cyclic test. Stiffness was assessed by the loading or unloading terms, k_l and k_u defined by Rimoy *et al.* (2013). Fig. 17 a) shows the loading stiffness trends, normalised by the first cycle value, for the four unfailed tests. Two of these showed k_l and k_u increasing consistently under cycling and reaching gains of up to 30% at $N = 1000$. The two other “unfailed” tests showed stiffness reducing up to 200 cycles, before increasing to reach almost 1.05 times the initial value at $N = 1000$. Fig. 17 b) presents the two failed tests’ trends: DP1-CY2 showed stiffness degrading from the first cycle falling by over 60% prior to final failure. Degradation was less marked in DP5-CY2 initially, but reached a similar level before final cyclic failure. As expected, stiffness degradation was generally slightly more marked on re-loading than on un-loading so leading to displacement accumulation during cycling. Re-test DP4-CY2, completed 6 days after test DP4-CY1 and a subsequent tension test to failure, showed gentler degradation trends and more stable normalised behaviour (Fig. 17a) than the initial cyclic test at lower load levels. It appears that stiffness recovers and normalised resistance grows with time following cyclic or static failure.

Impact on tension capacity

The post-cyclic tension tests are summarised in Table 5. Those following the “unfailed” experiments DP4-CY1 and DP7-CY1 indicated relatively modest changes in capacity (5% increase and 14% reduction respectively) when compared to the static trends predicted by Eq 2. However, cyclic failure led to more marked losses of 24% and 43% following DP5-CY2 and DP1-CY2, respectively.

Cyclic stability criteria

Cyclic axial loading tests on piles driven in clays and sands show trends that have been classified as Stable, Metastable or Unstable: (Karlsrud *et al.*, 1986, Poulos, 1988, Jardine and Standing, 2000, Tsuha *et al.*, 2012, Jardine *et al.*, 2012). Jardine & Standing (2012) and Rimoy *et al.* (2013) applied working definitions in their interpretation of open tube piles driven in dense sand at Dunkirk that referred to both possible numbers of cycles N and rates of permanent cyclic displacement accumulation, with:

- **Stable (S):** No failure within 1000 cycles. Pile displacements accumulate slowly over hundreds of cycles and tend to stabilise with cycling, remaining below $0.01D$ and showing rates of change of less than $1\text{mm}/1000$

cycles and negligible loss of cyclic stiffness. Cycling in this range does not affect foundation serviceability or reduce operational shaft capacity;

- **Unstable (US):** pile displacements accumulate rapidly leading to cyclic failure at $N < 100$ with either accumulated displacements greater than $0.1D$ or a rate of accumulation of displacement greater than $1\text{mm}/10$ cycles. The foundations may become unserviceable and potentially suffer marked reductions in operational shaft capacity;
- **Metastable (MS):** transitional behaviour where cycling may lead to failure with $100 < N < 1000$ and pile displacements developing at moderate rates over tens to hundreds of cycles without stabilisation. Serviceability and operational shaft capacity losses depend on numbers of cycles applied. Displacements of $0.01D$ to $0.1D$ develop at rates between $1\text{mm}/1000$ cycles and $1\text{mm}/10$ cycles.

Table 5 lists the outcomes of the cyclic loading tests. Applying the above categories, two of the tests (DP1-CY2, DP5-CY2) are unstable. The remaining four (DP1-CY1, DP4-CY1, DP5-CY1 DP7-CY1) classify as stable in terms of reaching 1000 cycles without failure or significant loss in operational tension capacity, but meta-stable with regards to accumulated displacements. The transition between unstable and metastable or stable behaviour appears to be abrupt. Fully stable behaviour was not observed, except in test DP4-CY2, which had been pre-failed, within the limited region of the interactive diagram that could be explored. Bearing in mind the tests involved purely one way loading at $UR \geq 0.48$, the stable region of behaviour appears to be more limited than was found, for example, by Jardine and Standing (2012) for Dunkirk sand. Jardine *et al.* (2012) emphasise that higher cyclic Q_{cyc}/Q_t amplitudes are likely to have a greater impact in two-way loading tests conducted with maximum loads set to achieve the same UR values; UR is not an adequate parameter on its own to characterise cyclic loading.

Permanent accumulated displacements

Under the limited range investigated, the virgin piles' permanent displacement accumulation trends correlate with UR. The unstable tests showed different accumulated displacement trends; test DP1-CY2 subjected to cyclic and average loads equivalent to a 'static' UR of 0.79, accumulated displacements of 2.3 to 3.4mm from its start and failed in 5 cycles. Displacement accumulation was more gradual in unstable test DP5-CY2 (under a 'static'

UR of 0.70) remaining below 0.1mm/cycle for the first 9 cycles, before more rapid accumulation led to failure in 32 cycles.

Three of the four Stable/Meta-stable tests (DP1-CY1, DP5-CY1 and DP7-CY1) exhibited consistent behaviour when subjected to cycling at loads equivalent to $0.48 < UR < 0.58$. While their displacement accumulation rates may have stabilised eventually, they followed the power law function given as Eq. 3 over $20 < N < 1000$, with coefficients A and B of 0.0015 ± 0.0004 and 0.32 ± 0.03 respectively; see Fig. 18. The remaining MS/S test (DP4-CY1), whose loads implied an equivalent static UR of 0.70, followed a steeper power law trend ($A = 0.0008$, $B = 0.49$) that may have accelerated and led to eventual failure if cycling had continued. The global trends must reflect locally progressive top-down degradation (Jardine *et al.*, 2012) that can only be checked through the use of local instrumentation. The coefficient A, can therefore be expected to vary with chalk profile, pile shaft length and cross section.

Finally, Fig. 19 shows the permanent displacements plotted on cyclic stability interaction diagrams, considering cases with $N = 3, 10, 20, 100, 300$ and 600. Contours are indicated for s_{acc}/D ratios of 0.2%, 0.5% and 2.0% for these one way cyclic tests. Further tests are required to examine potential pile scale effects and the influence of high-level two-way loading.

CONCLUSIONS

Improved guidance is required urgently to help design a wide range of wind-energy and other structures that are founded on piles driven in chalk. This paper reports programmes of static and cyclic loading tests on open steel tubes driven in low-medium density chalk that showed:

1. Notably low shaft resistances during driving along their main shaft lengths;
2. A strong dependence of local shaft resistance on relative distance above the pile tip (h/R);
3. Marginally lower average shaft driving resistances than the CIRIA static design guidance values;
4. Static tension capacities increasing markedly after driving. Gains exceeding 500% were interpreted after eight months, leading to average shaft stresses that exceeded the low-medium density guidance value by a factor of 4.3;

5. A hyperbolic shaft capacity trend with time that was 83% complete 100 days after installation. A single re-test conducted 8 months after one pile's first static failure showed a positive ageing trend, although its capacity fell well below that of the undisturbed piles;
6. Driving remoulded the chalk, creating a putty zone and probably very high excess pore pressures near to the pile tip. Rapid excess pore water pressure dissipation during and after driving led to markedly lower water contents close to the shaft;
7. Short-term reconsolidation that was too rapid to explain, on its own, the observed long-term increases in shaft capacity. Mechanisms involving early consolidation of chalk putty (contemporaneously with pile driving) followed by creep of radial effective stresses may provide explanations for the observed ageing trends, taken in combination with potential re-cementing and the redox chemical reactions that were noted to have occurred close to the pile shafts;
8. A range of responses to axial cyclic testing around 250 days after driving. One-way (non-dynamic) cycling that involved equivalent 'static' utilisation ratios > 0.70 led to clearly unstable behaviour with rapid accumulation of displacement, stiffness loss, failure in far less than 100 cycles and marked degradation in operational shaft capacity. One-way tests conducted with $0.48 < UR < 0.70$ led to broadly stable capacities and cyclic stiffness remaining constant or growing as cycling continued. However, the piles' accumulated displacement trends did not stabilise within 1000 cycles, suggesting only meta-stability. Greater degradation can be expected at the same UR values under high-level two-way loading;
9. The permanent displacement accumulation trends followed under the stable/metastable tests developed proportionally with N , raised to an exponent of $\approx 1/3$ that appeared to be insensitive to the loading parameters within the limited range (one-way $0.48 < UR < 0.70$) considered. Higher exponents applied in the unstable range. Further investigation is required to explore the potential effects of pile scale and chalk density, as well as the cyclic response under a wider range of cyclic loading conditions;
10. The experiments provide the first systematic study of which the Authors are aware into the effects of undisturbed ageing and cyclic loading of previously unfailed piles driven in chalk. Overall, guidance based on driving monitoring and early age tests is shown to be potentially highly conservative, while cyclic tests on aged piles showed responses that varied between stable and unstable, depending on the loading conditions. Potential predictive tools, which range from purely empirical global approaches through to

fully numerical analysis with advanced constitutive models, may now be tested against the reported field measurements.

ACKNOWLEDGEMENTS

This study is part of a joint industry project led by Pedro Barbosa that is funded by Innovate UK (formerly the Technology Strategy Board), Iberdrola/Scottish Power Renewables and supported by the Geotechnical Consulting Group, London. The Authors acknowledge the additional financial help and support received from Atkins for this work. The Authors also acknowledge colleagues from Imperial College: Dr. James Lawrence who guided the pile exhumation inspections and Emil Ushev and Tingfa Liu who helped conduct the pile tests. The Authors are also grateful to Professor Mark Randolph for the use of IMPACT, Dr. Francesca Ciavaglia and Dr. John Carey of Wind Support Ltd for providing supporting information on the site, and to Fugro Geoconsulting Ltd who carried out the laboratory testing.

APPENDIX A – TRIAXIAL TEST RESULTS

Further results from triaxial tests conducted in the Fugro commercial laboratory on samples from the site are shown on Figs 20 and 21. Fig. 20 shows the effective stress paths and stress-strain behaviour of consolidated undrained triaxial compression tests on remoulded samples, as consolidated both isotropically and under K_0 conditions. Fig. 21 presents the stress-strain behaviour observed during drained triaxial compression tests on intact samples. The axial strains shown in Fig. 20 and 21 are interpreted from the Fugro results, and show average local strain measurements (made with Hall effect gauges) plotted as solid lines up to the points where the sensors become less reliable than the external strain measurements, which were adopted to construct the later stage stress-strain curves and are plotted as dashed lines. A key point to note is the marked brittleness shown by the drained test on intact samples after they reached peak deviator stress at relatively small strains (<0.2%).

APPENDIX B – SUMMARY OF SIGNAL MATCHING ANALYSIS

Back analysis of the force and velocity signals measured near the pile head was undertaken to obtain static capacity employing IMPACT (Randolph, 2008), a signal matching program which includes models for soil resistance at the base and shaft based on elasto-dynamic theory (Randolph and Simons, 1986, Deeks and Randolph, 1995). The paragraphs below provide a brief description of the models used in the analyses.

The shaft model is based on the analytical solution for the dynamic load transfer stiffness of an elastic soil acting on the shaft of a rigid, long pile under vertical vibration (Novak *et al.*, 1978). Conditions at the pile soil interface are simulated by a viscous dashpot in parallel with a plastic slider and the far field is modelled with an elastic spring and a dashpot which represents radiation damping. The shear resistance in the far field is given by:

$$\tau = G \left[\frac{w}{D} + \frac{v_p}{V_s} \right] \quad \text{Eq. 4}$$

where w is displacement, v_p is particle velocity in the pile, D is the pile diameter, G is the shear modulus and V_s is the shear wave velocity ($V_s = \sqrt{G/\rho_s}$), where ρ_s is the soil mass density). A limiting shaft resistance is used to model the interface, expressed as a function of the relative velocity between the pile and the soil:

$$\tau_{\text{inter}} = \tau_s (1 + \alpha(\Delta v/v_0)^\beta) \quad \text{Eq. 5}$$

where τ_s is the static resistance of the pile, v_0 is equal to 1 m/s, Δv is the relative velocity between pile and soil and α and β are empirical viscosity parameters. IMPACT includes implicit modelling of the internal as well as external shaft resistance, with the internal soil modelled in a similar manner to Eq. 4 and 5. The Deeks and Randolph (1995) base model is similar to the shaft model described with the exception of lumped masses connected to the pile and a supplementary radiation dashpot. The resistance at the pile base is represented by:

$$Q_b = \frac{4GR}{1 - \mu} w + \frac{3.2R^2 \sqrt{G\rho_s}}{1 - \mu} v_p \quad \text{Eq. 6}$$

The lumped mass is represented by:

$$m_0 = 1.28R^3 \rho_s \quad \text{Eq. 7}$$

Where μ is Poisson's ratio and R is the pile radius. The plastic slider is limited to the static end bearing capacity, $q_{b,\text{lim}}$ entered by the user. No allowance is made for viscous effects at the pile base.

The measured pile force and pile velocity times impedance, Z measured at the pile head were used as input to the program and signal matching was carried out by comparison of the calculated and measured upward travelling waves. The remaining inputs are shear modulus, soil density, limiting internal and external shaft resistance and base resistance. The Authors' initial trial parameter sets were gauged from the site investigations described in the main text. Consistent with the approach adopted by Salgado *et al.* (2015) the shear modulus used in the analyses was the secant modulus, G_1 at values degraded from the small strain (G_{max}) equivalent to $\approx 20\% G_{max}$. Fig. 22 shows the partial measured and calculated velocity and force time histories from a typical result. The average external compressive shaft load at EoD was 39.3kN.

NOTATION

Roman Alphabet

A, B	Power law parameters
c'	Cohesion intercept
c_h	Coefficient of radial consolidation
$c_{h,NC}$	Coefficient of radial consolidation under normally consolidated conditions
$c_{h,OC}$	Coefficient of radial consolidation under overconsolidated conditions
$c_{h,piezo}$	Operational coefficient of radial consolidation during CPTu dissipation tests
D	Diameter of pile or penetrometer
f_s	CPT sleeve friction
G	Shear modulus
G_s	Particle density
G_{max}	Maximum shear modulus
G_1	Secant shear modulus
h	Distance from the pile tip
I_p	Plasticity index
k_l	Cyclic loading stiffness
k_s	Displacement creep rate
k_u	Cyclic unloading stiffness
m	Empirical factor describing hyperbolic ageing trend
m_0	Lumped mass
N	Number of cycles
$q_{b,lim}$	Limit base resistance
q_c	CPT cone resistance
q_u	Unconfined compressive strength
Q_b	Pile base capacity
Q_{cyc}	Axial cyclic load amplitude

Q_{mean}	Mean axial cyclic load
Q_t	Current pile capacity in tension
$Q_{t(\text{EOD})}$	Static compressive tension capacity at EoD from dynamic tests
Q_u	Ultimate equalised pile capacity in tension
r	Distance from the pile centre
R	Pile radius
R_{cptu}	CPTu radius
R^*	Open ended pile effective radius
S_{acc}	Accumulated permanent cyclic displacement
S_r	Degree of saturation
t	Time
t_{pile}	Pile wall thickness
t_{zone}	Thickness of the zone surrounding the pile shaft
t_{50}	Time for 50% dissipation of excess pore water pressures in a CPT dissipation test
T_{50}	Time for 50% set up of ultimate capacity Q_u
u_2	CPTu pore pressure measured at the u_2 position
v	Velocity of the pile or penetrometer
v_p	Particle velocity
Δv	Relative velocity between pile and soil
V	Dimensionless velocity
V_s	Shear wave velocity
w	Displacement in the z direction
w_c	Moisture content
w_l	Liquid limit
w_p	Plastic limit
z	Depth below ground level
Z	Pile impedance

Greek alphabet

α, β	Empirical viscosity parameters
δ_r	Residual interface friction angle
μ	Poisson's ratio
ρ_s	Soil mass density
τ_{rz}	Total shaft resistance
τ_s	Static shaft resistance in back analysis of dynamic tests
τ_{lim}	Limit dynamic static shaft resistance
φ'	Effective angle of shearing resistance

REFERENCES

- Andersen, K. H., Puech, A. & Jardine, R. J. (2013). Cyclic resistant geotechnical design and parameter selection for offshore engineering and other applications. In *Proc. TC 209 Workshop - 18th Int. Conf. Soil. Mech. Geotech. Eng.: 'Design for cyclic loading: piles and other foundations'* (Puech, A., (ed)). Paris, France, pp. 9-44: Presses des Ponts
- Barbosa, P., Geduhn, M., Jardine, R. J., Schroeder, F. C. & Horn, M. (2015). Offshore pile load tests in chalk. In *Proc. 16th Eur. Conf. Soil Mech. & Geotech. Eng.* (Winter, M. G., (ed)). Edinburgh, Scotland, pp. 2885-2890: ICE Publishing
- Bogard, J. D. & Matlock, H. (1990). Application of model pile tests to axial pile design. In *Proc. 22nd Offshore Technology Conference*, Houston, Texas, pp. 271-278: Offshore Technology Conference
- Bond, A. J. & Jardine, R. J. (1991). Effects of installing displacement piles in a high OCR clay. *Géotechnique*, **41**, No. 3, 341-363.
- Bowden, A. J., Spink, T. W. & Mortimore, R. N. (2002). The engineering description of chalk: its strength, hardness and density. *Q. J. Eng. Geol. Hydrogeol.*, **35**, No. 4, 355-361.
- Buckley, R. M. (2014). *Axial cyclic loading of piles in sand*. MSc Thesis, Imperial College London, London, UK
- Bundy, S. P. S. (2013). *Geotechnical properties of chalk putties*. PhD Thesis, University of Portsmouth, Portsmouth, UK
- Burland, J. B. & French, D. J. (1990). Results of trials in weathered chalk of a novel piling system – the wedge pile. In *Proc. Intl. Chalk Symp.* (Burland, J. B. et al., (eds)). Brighton, UK pp. 375-383: Thomas Telford
- Carrington, T. M., Li, G. & Rattley, M. J. (2011). A new assessment of ultimate unit friction for driven piles in low to medium density chalk. In *Proc. 15th Eur. Conf. Soil Mech. & Geotech. Eng.* (Anagnostopoulos, A. et al., (eds)). Amsterdam, The Netherlands, pp. 825-830: IOS Press
- Cassidy, M. J. (2012). Experimental observations of the penetration of spudcan footings in silt. *Géotechnique*, **62**, No. 8, 727-732.
- Chow, F. C. (1997). *Investigations into Displacement Pile Behaviour for Offshore Foundations*. PhD Thesis, Imperial College London, London, UK
- Ciavaglia, F., Carey, J. & Diambra, A. (2017a). Monotonic and cyclic lateral tests on driven piles in Chalk. *Proc. of the ICE Geotech. Eng.*, **0**, No. 0, 1-14.
- Ciavaglia, F., Carey, J. & Diambra, A. (2017b). Time-dependent uplift capacity of driven piles in low to medium density chalk. *Géotechnique Letters* 7. March, 1-7
- Clayton, C. R. I. (1978). *Chalk as Fill*. PhD Thesis, University of Surrey, Surrey, UK
- Clayton, C. R. I., Matthews, M. C. & Heymann, G. (2002). The Chalk. In *Proc. 1st Intl. Workshop on Characterisation and Engineering Properties of Natural Soils* (Tan, T. S. et al., (eds)). Singapore, pp. 1403-1434: CRC Press
- Deeks, A. J. & Randolph, M. F. (1995). A simple model for inelastic footing response to transient loading. *Int. J. Num. Meth. Geotech. Eng.*, **19**, No. 5, 307-329.
- Diambra, A., Ciavaglia, F., Dimelow, C., Carey, J. & Nash, D. F. T. (2014). Performance of cyclic cone penetration tests in chalk. *Géotechnique Letters* 4. July–September, 230-237
- Doherty, P., Gavin, K. & Casey, B. (2011). The geotechnical challenges facing the offshore wind sector. In *Proc. of Geo-Frontiers 2011: Advances in Geotechnical Engineering* (Han, J. et al., (eds)). Dallas, Texas, pp. 162-171: ASCE
- Dührkop, J., Augustesen, A. H. & Barbosa, P. (2015). Cyclic pile load tests combined with laboratory results to design offshore wind turbine foundations in chalk. In *Poc. Conf. Frontiers in Offshore Geotechnics III (ISFOG)* (Meyer, V., (ed)). Oslo, Norway, pp. 533-538: CRC Press

- Ea-Pfähle 2014. *Recommendations on Piling: Piling Committee of the German Geotechnical Society (abbreviated as: EA Pfähle)*, Germany: John Wiley & Sons.
- Fahey, M. & Lee Goh, A. (1995). A comparison of pressuremeter and piezocone methods of determining the coefficient of consolidation. In *Proc. 4th Intl. Symp. on the Pressuremeter and Its New Avenues* (Ballivy, G., (ed)). Quebec, Canada, pp. 153-60: Balkema
- Finnie, I. M. S. & Randolph, M. F. (1994). Punch-through and liquefaction induced failure of shallow foundations on calcareous sediments. In *Proc. Int. Conf. Behavior of Offshore Structures* (Chrysostomidis, C., (ed)). Boston, Massachusetts, pp. 217-230: Pergamon
- Fugro (2012). *Laboratory testing report: Pile test site, chalk specific testing. St. Nicholas at Wade, UK, D34001-2*.
- Gavin, K., Jardine, R. J., Karlsrud, K. & Lehane, B. M. (2015). The effects of pile ageing on the shaft capacity of offshore piles in sand. In *Proc. Conf. Frontiers in Offshore Geotechnics III (ISFOG)*, Oslo, Norway, pp. 129-151: CRC Press
- Hancock, J. M. (1975). The petrology of the Chalk. *Proceedings of the Geologists' Association*, **86**, No. 4, 499-535.
- Heerema, E. P. (1978). Predicting pile driveability: heather as an illustration of the friction fatigue theory. In *Proc. Eur. Offshore Petroleum Conf.*, London, UK, pp. 413-422: Society of Petroleum Engineers
- Hobbs, N. B. & Atkinson, M. S. (1993). Compression and tension tests on an open-ended tube pile in chalk. *Ground Engineering*, **26**, No. 3, 31-34.
- Jardine, R. J., Symes, M. J. & Burland, J. B. (1984). The measurement of soil stiffness in the triaxial apparatus. *Géotechnique*, **34**, No. 3, 323-340.
- Jardine, R. J. & Standing, J. R. (2000). *Pile Load Testing Performed for HSE Cyclic Loading Study at Dunkirk, France Volume 1 & 2*, OTO2000 007.
- Jardine, R. J., Chow, F. C., Overy, R. & Standing, J. R. 2005a. *ICP design methods for driven piles in sands and clays*, London: Thomas Telford.
- Jardine, R. J., Standing, J. R. & Kovacevic, N. (2005b). Lessons learned from full scale observations and the practical application of advanced testing and modeling. In *Proc. 3rd Int. Symp. on Deformation Characteristics of Geomaterials* (Di Benedetto, H. et al., (eds)). Lyon, France, pp. 201-245: Balkema
- Jardine, R. J., Standing, J. R. & Chow, F. C. (2006). Some observations of the effects of time on the capacity of piles driven in sand. *Géotechnique*, **56**, No. 4, 227-244.
- Jardine, R. J., Puech, A. & Andersen, K. H. (2012). Cyclic loading of offshore piles: potential effects and practical design. In *Proc. 7th Int. Conf. on Offshore Site Investigation and Geotechnics* (Allan, P. et al., (eds)). London, UK, pp. 59-97: Society for Underwater Technology (SUT)
- Jardine, R. J. & Standing, J. R. (2012). Field axial cyclic loading experiments on piles driven in sand. *Soils Found.*, **52**, No. 4, 723-736.
- Jardine, R. J., Zhu, B. T., Foray, P. & Yang, Z. X. (2013). Interpretation of stress measurements made around closed-ended displacement piles in sand. *Géotechnique*, **63**, No. 8, 613-627.
- Jardine, R. J. (2017). Geotechnics and Energy: 56th Rankine Lecture. *Géotechnique, to appear*.
- Karlsrud, K., Nadim, F. & Haugen, T. (1986). Piles in clay under cyclic axial loading - Field tests and computational modelling. In *Proc. 3rd. Int. Conf. on Numerical Methods in Offshore Piling* (Du Petrole, F., (ed)). Nantes, France, pp. 165-190: Editions Technip
- Karlsrud, K., Jensen, T. G., Lied, E. K. W., Nowacki, F. & Simonsen, A. S. (2014). Significant ageing effects for axially loaded piles in sand and clay verified by new field load tests. In *Proc. 46th Offshore Technology Conference*, Houston, Texas, pp. 1-19: Offshore Technology Conference
- Lahrs, T. & Kallias, A. (2013). Probebelastungen von Stahlrohren in Kreide für den Offshore-Windpark Baltic 2. In *Proc. Pfahl Symposium*, Braunschweig, Germany, pp. 451-466: Pfahl Symposium
- Le, T. M. H., Eiksund, G. R., Strøm, P. J. & Saue, M. (2014). Geological and geotechnical characterisation for offshore wind turbine foundations: A case study of the Sheringham Shoal wind farm. *Engineering Geology*. 2014, 40-53

- Lehane, B. M. & Jardine, R. J. (1992a). The Behavior of a Displacement Pile in Glacial Till. In *Proc. 6th Int. Conf. Behavior of Offshore Structures* (Patel, M. H. et al., (eds)). Imperial College, pp. 555-566: BPP Technical Services
- Lehane, B. M. & Jardine, R. J. (1992b). The behaviour of a displacement pile in Bothkennar clay. In *Proc. Wroth Memorial Symp. on Predictive Soil Mechanics* (Houlsby, G. T. et al., (eds)). Oxford, UK, pp. 421-435: Thomas Telford
- Lehane, B. M., Jardine, R. J., Bond, A. J. & Frank, R. (1993). Mechanisms of shaft friction in sand from instrumented pile tests. *J. Geotech. Eng-ASCE*, **119**, No. 1, 19-35.
- Leroueil, S., Demers, D., La Rochelle, P., Martel, G. & Virely, D. (1995). Practical applications of the piezocone in Champlain sea clays. In *Proc. Int. Symp. on Cone Penetration Testing*, Linköping, Sweden, pp. 515-522: Swedish Geotechnical Society
- Lim, J. K. & Lehane, B. M. (2014). Characterisation of the effects of time on the shaft friction of displacement piles in sand. *Géotechnique*, **64**, No. 6, 476-485.
- Lord, J. A., Clayton, C. R. I. & Mortimore, R. N. 2002. *Report C574: Engineering in chalk*, London, UK: CIRIA.
- Mesri, G., Feng, T. W. & Benak, J. M. (1990). Post densification penetration resistance of clean sands. *J. Geotech. Eng.*, **116**, No. 7, 1095-1115.
- Mortimore, R. N. (2012). The 11th Glossop Lecture: Making sense of Chalk: a total-rock approach to its Engineering Geology. *Q. J. Eng. Geol. Hydrogeol.*, 252-334
- Muir Wood, A., Mackenzie, B., Burbury, D., Rattley, M., Clayton, C. R. I., Mygind, M., Wessel Andersen, K., Le Blanc Thilsted, C. & Albjerg Liingaard, M. (2015). Design of large diameter monopiles in chalk at Westermøst Rough offshore wind farm. In *Proc. Conf. Frontiers in Offshore Geotechnics III (ISFOG)* (Meyer, V., (ed)). Oslo, Norway, pp. 723-728: CRC Press
- Norrie, C. (2015). *Pile driving performance in low to medium density chalk*. MSc Thesis, Imperial College London, London, UK
- Novak, M., Aboul-Ella, F. & Nogami, T. (1978). Dynamic soil reactions for plane strain case. *J. Eng. Mech. Div.*, **104**, No. EM4, 953-959.
- Poulos, H. G. (1988). Cyclic stability diagram for axially loaded piles. *J. Geotech. Geoenviron. Eng.*, **114**, No. 8, 877-895.
- Power, P. (1982). The use of the electric static cone penetrometer in the determination of the engineering properties of chalk. In *Proc. 2nd Eur. Symp. on Penetration Testing* (Verruijt, A. et al., (eds)). Amsterdam, The Netherlands, pp. 769-774: CRC Press
- Randolph, M., Dolwin, J. & Beck, R. (1994). Design of driven piles in sand. *Geotechnique*, **44**, No. 3, 427-48.
- Randolph, M. F. & Simons, H. A. (1986). An improved soil model for one-dimensional pile driving analysis. In *Proc. 3rd. Int. Conf. on Num. Meth. in Offshore Piling* (Du Petrole, F., (ed)). Nantes, France, pp. 3-17: Editions Technip
- Randolph, M. F. (2004). Characterisation of soft sediments for offshore applications. In *Proc. 2nd Int. Conf. on Site Characterisation* (Da Fonseca, V. et al., (eds)). Porto, Portugal, pp. 209-232: IOS Press
- Randolph, M. F. (2008). *IMPACT - Dynamic analysis of pile driving.*, Manual.
- Razoaki, R. N. (2000). *Effect of ageing on mechanics of chalk slurries*. PhD Thesis, University of Portsmouth, Portsmouth, UK
- Rimoy, S. P., Jardine, R. J. & Standing, J. R. (2013). Displacement response to axial cycling of piles driven in sand. *Proc. of the ICE Geotech. Eng.*, **166**, No. GE2, 131-146.
- Rimoy, S. P., Silva, M., Jardine, R. J., Yang, Z. X., Zhu, B. T. & Tsuha, C. H. C. (2015). Field and model investigations into the influence of age on axial capacity of displacement piles in silica sands. *Géotechnique*, **65**, No. 7, 576-589.
- Salgado, R., Loukidis, D., Abou-Jaoude, G. & Zhang, Y. (2015). The role of soil stiffness non-linearity in 1D pile driving simulations. *Géotechnique*, **65**, No. 3, 169-187.

- Setech (2007). *Trial site investigation - Thanet offshore wind farm trial site*, 8564/1.
- Skov, R. & Denver, H. (1988). Time-dependence of bearing capacity of piles. In *Proc. 3rd Int. Conf. on the Application of Stress-Wave Theory to Piles* (Niyama, S. et al., (eds)). Ottawa, Canada., pp. 879-888: Balkema
- Suzuki, Y. (2014). *Investigation and interpretation of cone penetration rate effects*. PhD Thesis, The University of Western Australia, Crawley, Australia
- Tan, S. L., Cuthbertson, J. & Kimmerling, R. E. (2004). Prediction of pile set-up in non-cohesive soils. *Current practices and future trends in deep foundations - ASCE, GSP*, No. 125, 50-65.
- Tsuha, C. H. C., Foray, P. Y., Jardine, R. J., Yang, Z. X., Silva, M. & Rimoy, S. (2012). Behaviour of displacement piles in sand under cyclic axial loading. *Soils Found.*, **52**, No. 3, 393-410.
- Vijayvergiya, V. N., Cheng, A. P. & Kolk, H. J. (1977). Design and installation of piles in chalk. In *Proc. 9th Offshore Technology Conf.*, Houston, Texas, pp. 459-464: Offshore Technology Conference
- White, D. J. (2005). A general framework for shaft resistance on displacement piles in sand. In *Proc. Conf. Frontiers in Offshore Geotechnics I (ISFOG)* (Gourvenec, S. et al., (eds)). Perth, Australia, pp. 697-703: CRC Press
- Yang, Z. X., Guo, W. B., Jardine, R. J. & Chow, F. C. (2016). Design method reliability assessment from an extended database of axial load tests on piles driven in sand. *Can. Geotech. J.*, **54**, No. 1, 59-74.
- Ziogos, A., Brown, M., Ivanovic, A. & Morgan, N. (2016). Chalk-steel interface testing for marine energy foundations. *Proc. of the ICE Geotech. Eng.* DOI: 10.1680/jgeen.16.00112. 0, 1-14

LIST OF TABLES

Table 1 Summary of classification and index tests from 0 to 7m depth (Setech, 2007, Fugro, 2012)

Table 2 Summary of pile test codes and test histories for ageing trends

Table 3 Summary of pile test codes and test histories for cyclic loading effects

Table 4 Post ageing and end of driving capacities of virgin piles in the static capacity study

Table 5 Summary of cyclic loading test outcomes

LIST OF FIGURES

Fig. 1 a) overall location of previous JIP site and current IC site b) plan showing layout of test piles and CPTus at the IC test site

Fig. 2 Typical site profile at the IC test site

Fig. 3 Peak failure envelopes interpreted from Consolidated Drained (CD) and Consolidated Undrained (CU) triaxial tests on intact and remoulded samples (data from Fugro, 2012)

Fig. 4 Section A-A: Cone resistance with depth at the IC test site (as shown on Fig. 1)

Fig. 5 Blow counts per 250mm versus average penetration depth for driven piles DP1 – DP7

Fig. 6 Profile of total EoD shaft resistance obtained by back analysis of the dynamic test results

Fig. 7 Schematic of conditions encountered during exhumation of piles DP1 and DP7

Fig. 8 Radial water content profiles with relative radial distance from the pile centre a) near and far field b) near field, normalised by pile outside radius R

Fig. 9 Schematic of test rig (not to scale) a) side view b) elevation

Fig. 10 Schematic illustration of cyclic loading waveform

Fig. 11 Load displacement curves from first time tension tests on DP2, DP3 and DP6.

Fig. 12 Shaft capacity growth with time for first time tension tests to failure on DP2, DP3 and DP6 and retest on DP2

Fig. 13 Global stiffness versus pile load for first time tension tests to failure on DP2, DP3 and DP6 and re-test on DP2

Fig. 14 Permanent accumulated cyclic displacement normalised by pile diameter for unfailed tests a) DP1-CY1 b) DP4-CY1 c) DP5-CY1 d) DP7-CY1 and e) retest DP4-CY2

Fig. 15 Permanent accumulated cyclic displacement normalised by pile diameter for failed tests

Fig. 16 Cyclic loading interaction diagram with number of cycles either to failure or to the end of the test if unfailed

Fig. 17 Global axial loading stiffness for tests for a) unfailed tests f b) failed tests

Fig. 18 Permanent displacement accumulation with cycles for metastable/unstable tests on natural scale with power law fits and parameters shown

Fig. 19 Cyclic interaction charts showing accumulated displacements (normalised by pile diameter) at a) $N=3$ b) $N=10$ c) $N=20$ d) $N=100$ e) $N=300$ and f) $N=60$

Fig. 20 Undrained triaxial tests on remoulded samples a) stress paths in q - p' space b) q - ϵ_{ax}

Fig. 21 Drained triaxial tests on intact samples

Fig. 22 Signal matching results for pile DP7 a) force and velocity times impedance b) pile head displacement

TABLES

Table 1 Summary of classification and index tests from 0 to 7m depth (Setech, 2007, Fugro, 2012)

Test type	Range (Mean)
Intact dry density, IDD (Mg/m^3)	1.38 – 1.64 (1.49)
Natural moisture content, w_c (%)	28 – 33 (29.9)
Degree of saturation, S_r (%)	90 - 100
Liquid limit, w_l (%)	30 – 31 (30.6)
Plasticity index, I_p (%)	5 – 8 (6.4)
Unconfined compressive strength, q_u (MPa)	2.1
Particle density, G_s (Mg/m^3)	2.71

Table 2 Summary of pile test codes and test histories for ageing trends

Test pile	Test code ¹	Pile Age (days)	Comment
DP2	DP2-T1	10	Static test on previously untested pile
	DP2-T2	227	Static test on a previously failed pile
DP3	DP3-T1	106	Static test on previously untested pile
DP6	DP6-T1	246	Static test on previously untested pile

1. The test code nomenclature refers to the pile number (e.g. DP1), then the test type (CY = cyclic, T = first time static tension TPC = post cyclic static tension) and the number of experiments previously completed up to and including that test.

Table 3 Summary of pile test codes and test histories for cyclic loading effects

Test pile	Test code ¹	Pile Age (days)	Mode	Comment
DP1	DP1-CY1	253	Cyclic	Low level cyclic test on previously untested pile
	DP1-CY2	253	Cyclic	Second cyclic test immediately after DP1-CY1
	DP1-TPC	253	Static	'Quick' static test post cyclic failure
DP4	DP4-CY1	249	Cyclic	Low level cyclic test on previously untested pile
	DP4- TPC	249	Static	'Quick' static test post DP4-CY1
	DP4-CY2	255	Cyclic	Second cyclic test on DP4 (Retest)
DP5	DP5-CY1	254	Cyclic	Low level cyclic test on previously untested pile
	DP5-CY2	254	Cyclic	Second cyclic test immediately after DP5-CY1
	DP5-TPC	254	Static	'Quick' static test post cyclic failure
DP7	DP7-CY1	247	Cyclic	Cyclic test on previously untested pile
	DP7- TPC	247	Static	'Quick' static test post cyclic failure

1. The test code nomenclature refers to the pile number (e.g. DP1), then the test type (CY = cyclic, TPC = post cyclic static tension) and the number of experiments previously completed up to and including that test.

Table 4 Post ageing and end of driving capacities of virgin piles in the static capacity study

Test code	Age (days)	Shaft Capacity ¹ (kN)	Shaft Resistance ² (kPa)	Capacity Change ³ (%)
DP2-T1	10	94	39	+239
DP3-T1	106	186	77	+473
DP6-T1	246	206	86	+524

1. Includes correction for pile and soil self weight
2. External - only external shaft resistance is assumed to be mobilised during a static tension test
3. Calculated based on average external compressive shaft capacity from three DLT results (= 39.3kN)

Table 5 Summary of cyclic loading test outcomes

Test code	One way axial cyclic loading									Post cyclic axial tension loading	
	Q_{min} (kN)	Q_{max} (kN)	Q_t (kN) ¹	Q_{cyc}/Q_t (-)	Q_{mean}/Q_t (-)	UR^2 (-)	Period T (s)	No. of cycles ³	Class	Q_{pc} (kN)	Capacity change (%) ⁴
DP1-CY1 ⁵	40	103	207.6	0.15	0.34	0.50	15	>1059	MS/S	-	-
DP1-CY2	40	164	207.6	0.30	0.49	0.79	30	5	US	117.6	-43
DP4-CY1	82	145	207.4	0.15	0.55	0.70	15	>1004	MS/S	216.8	+5
DP4-CY2 ⁵	49	146	207.8	0.23	0.47	0.70	20-30	>1003	S	-	-
DP5-CY1	4	99	207.7	0.23	0.25	0.48	15	>1000	MS/S	-	-
DP5-CY2	5	146	207.7	0.34	0.36	0.70	30	32	US	158.4	-24
DP7-CY1	24	120	207.3	0.23	0.35	0.58	30	>1000	MS/S	177.9	-14

1. Reference capacity Q_t at the time of the test calculated from Eq. 2.
2. UR = Utilisation Ratio = Q_{max}/Q_t
3. prefix ">" : no cyclic failure when number of cycles reached
4. When compared to Q_t
5. Marginally higher cyclic loads were applied initially than intended for three cycles; these have not been included in the cycle number or permanent displacement trends
6. Re-test on a pile previously failed in static tension and subjected to cyclic loading
7. All loads given in Table are net loads (measured load less pile and chalk self weight)

FIGURES

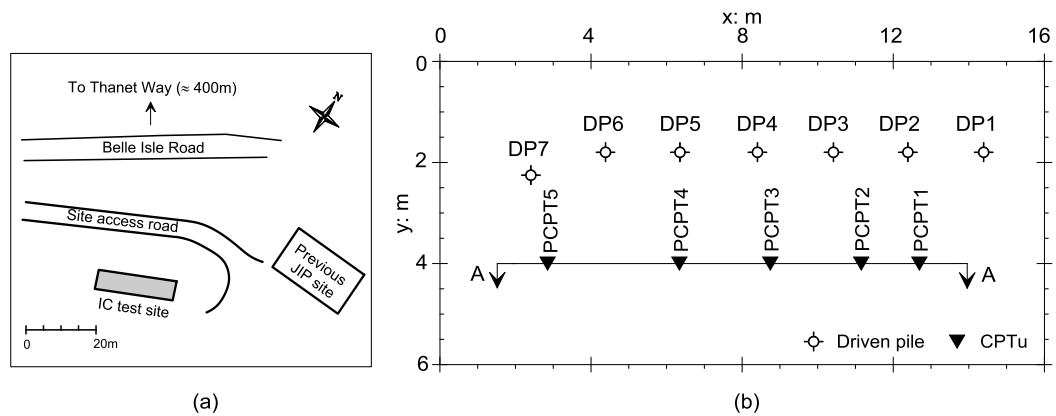


Figure 1 a) overall location of previous JIP site and current IC site b) plan showing layout of test piles and CPTus at the IC test site

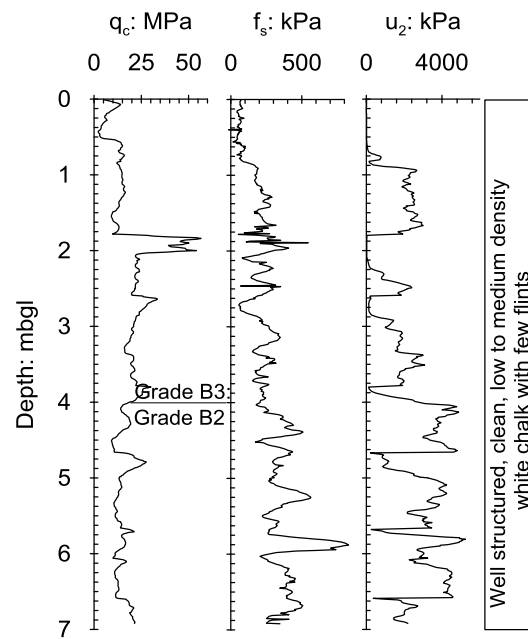


Figure 2 Typical site profile at the IC test site

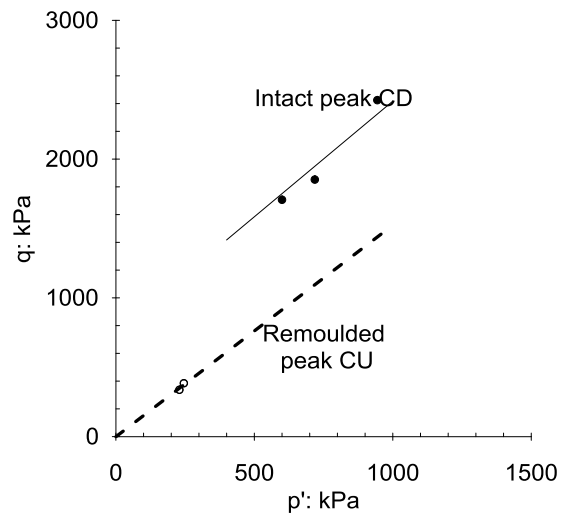


Figure 3 Peak failure envelopes interpreted from Consolidated Drained (CD) and Consolidated Undrained (CU) triaxial tests on intact and remoulded samples (data from Fugro, 2012)

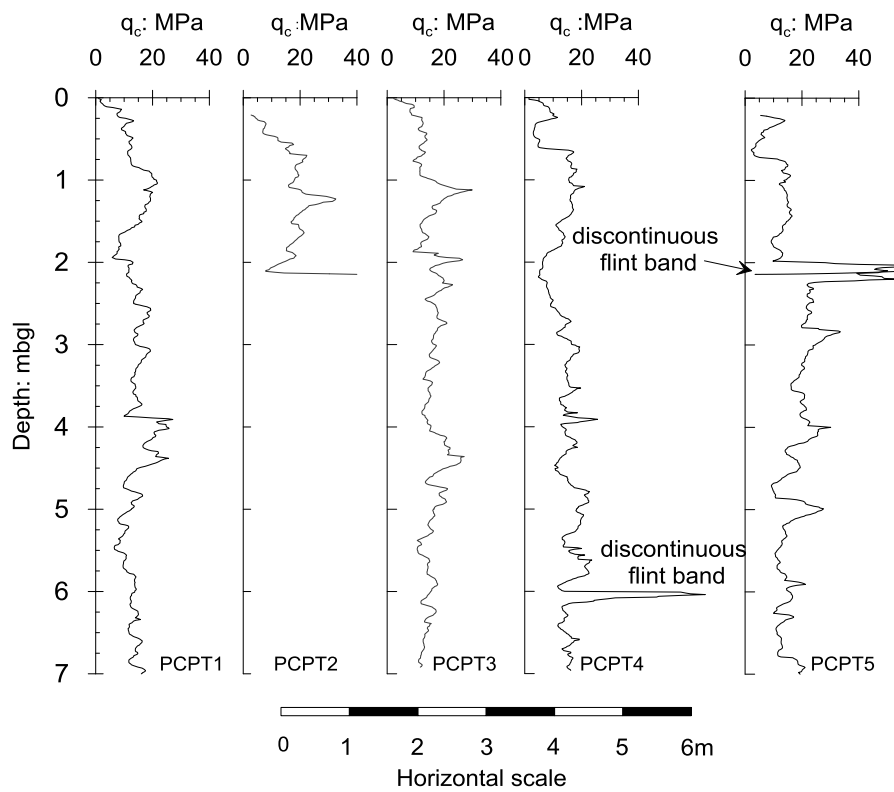


Figure 4 Section A-A: Cone resistance with depth at the IC test site (as shown on Figure 1)

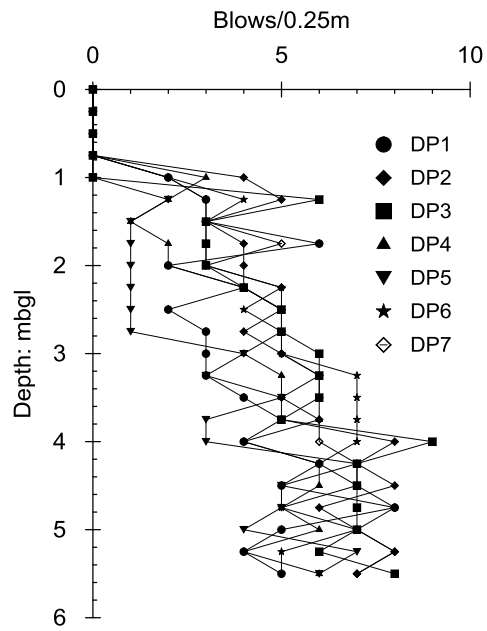


Figure 5 Blow counts per 250mm versus average penetration depth for driven piles DP1 – DP7

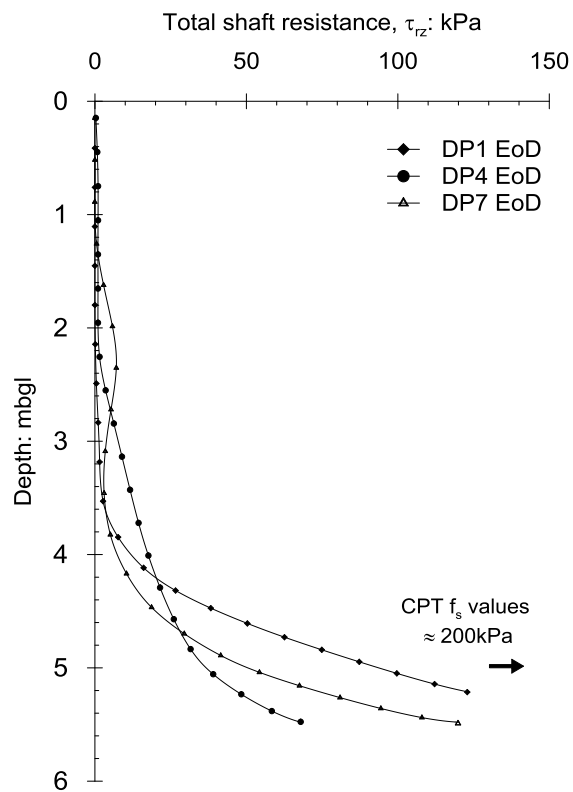


Figure 6 Profile of total EoD shaft resistance obtained by back analysis of the dynamic test results

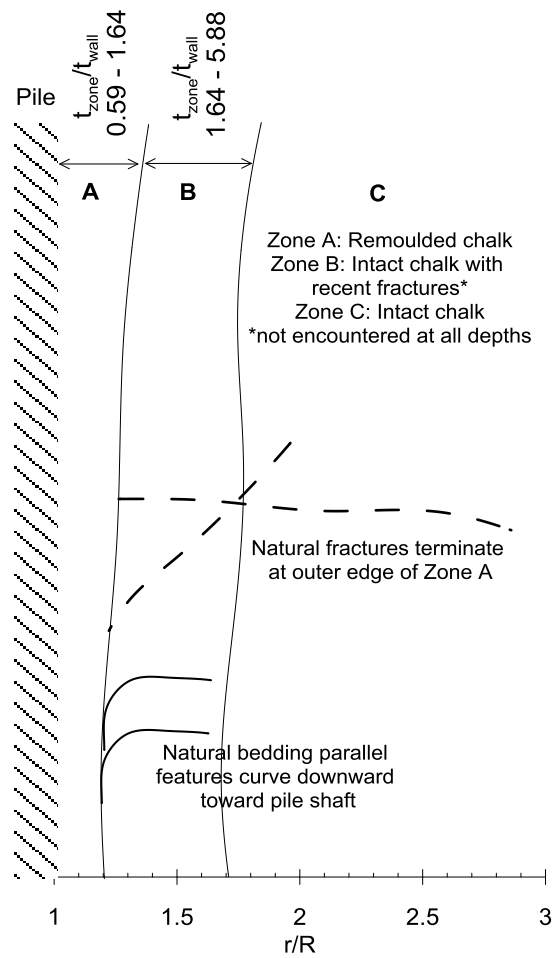


Figure 7 Schematic of conditions encountered during exhumation of piles DP1 and DP7

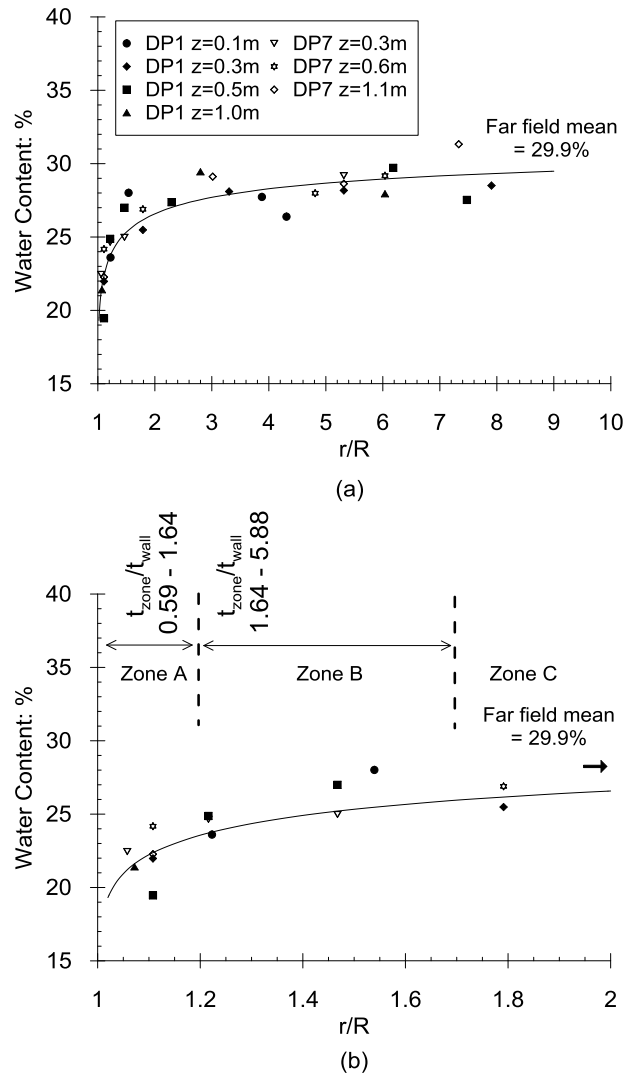


Figure 8 Radial water content profiles with relative radial distance from the pile centre a) near and far field b) near field, normalised by pile outside radius R

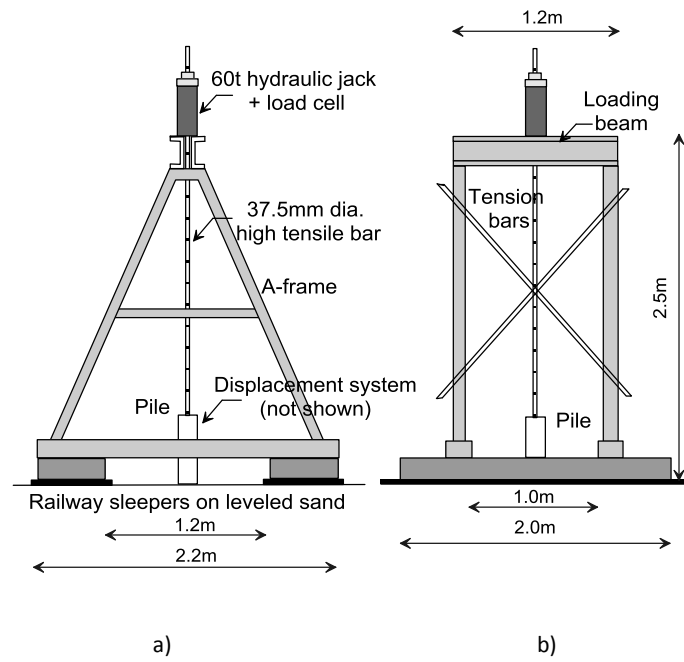


Figure 9 Schematic of test rig (not to scale) a) side view b) elevation

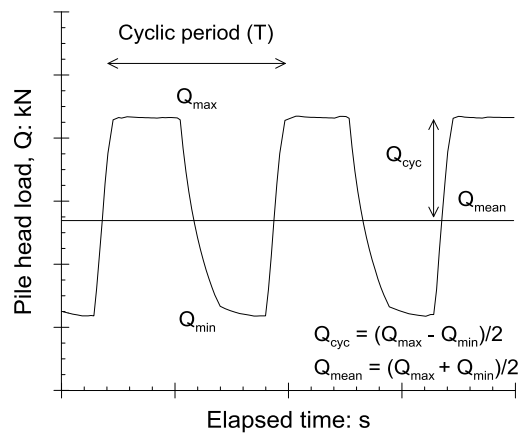


Figure 10 Schematic illustration of cyclic loading waveform

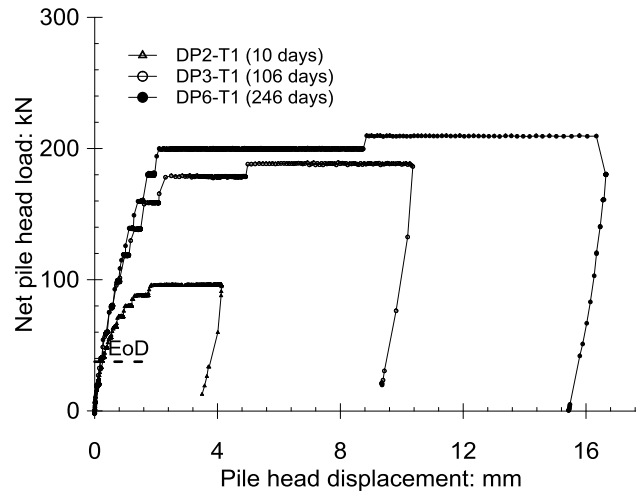


Figure 11 Load displacement curves from first time tension tests on DP2, DP3 and DP6.

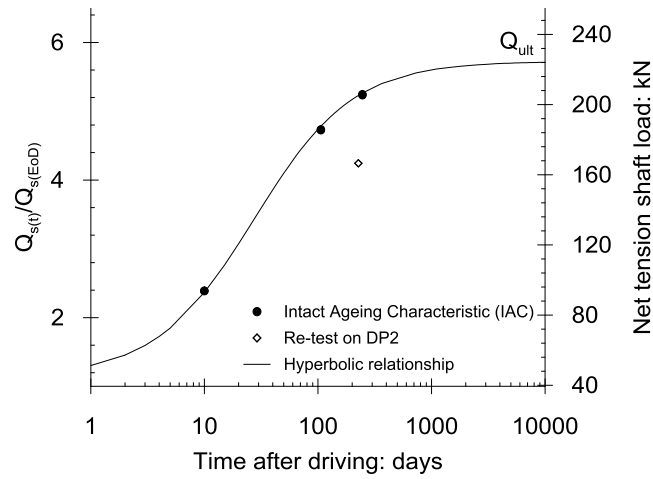


Figure 12 Shaft capacity growth with time for first time tension tests to failure on DP2, DP3 and DP6 and retest on DP2

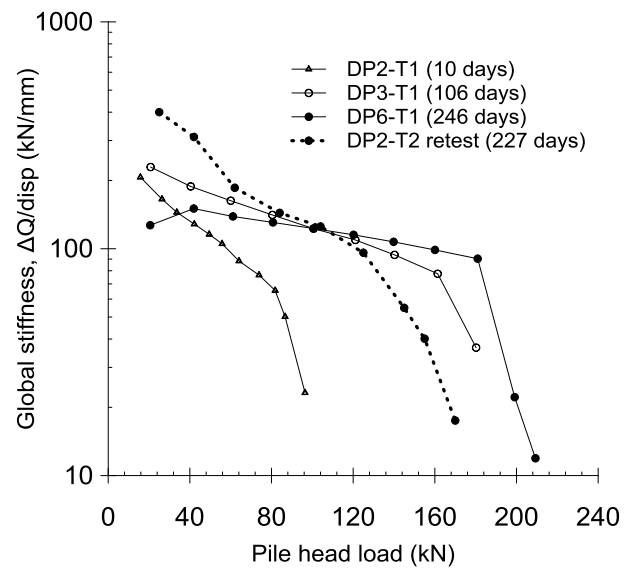


Figure 13 Global stiffness versus pile load for first time tension tests to failure on DP2, DP3 and DP6 and re-test on DP2

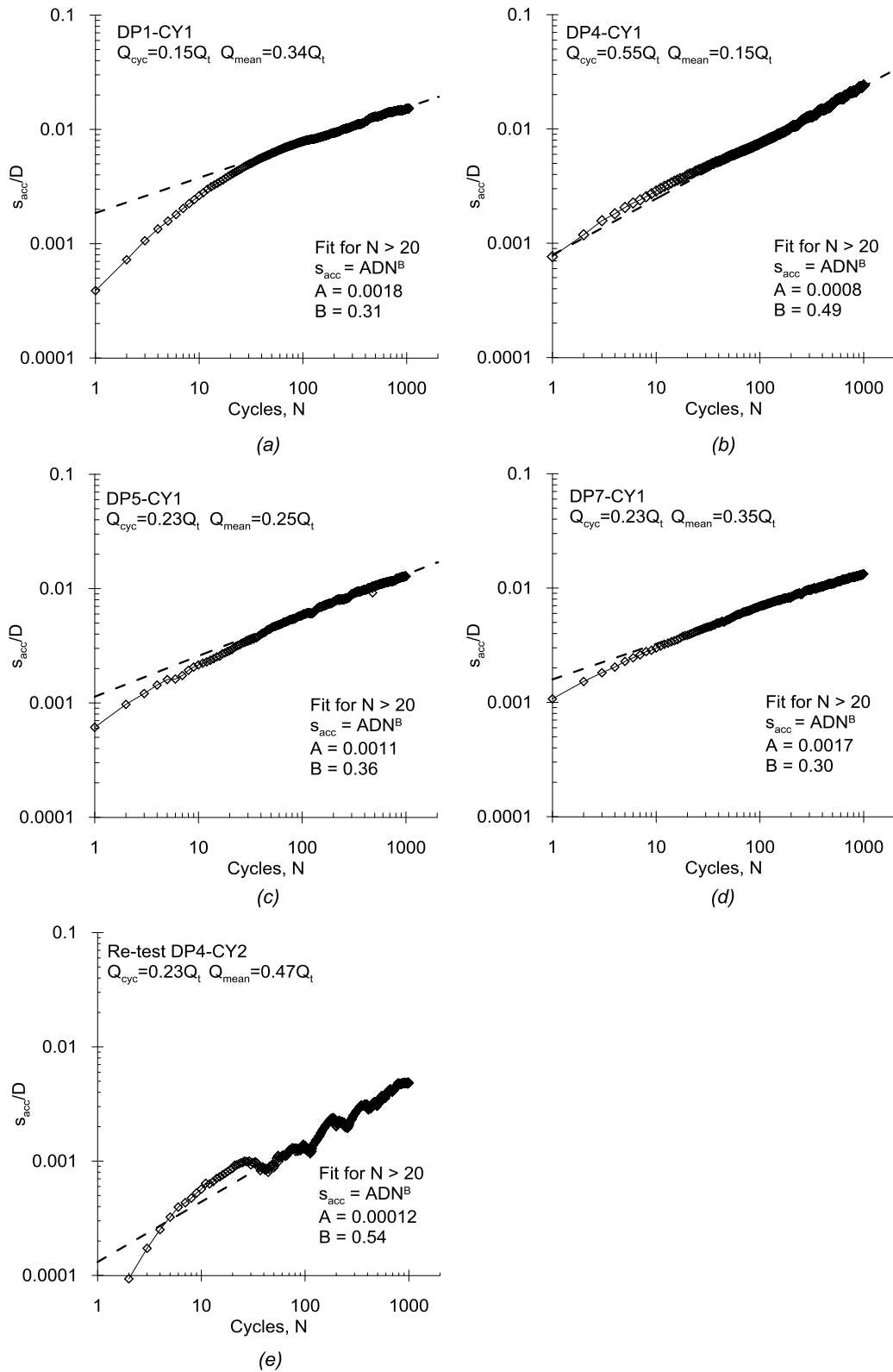


Figure 14 Permanent accumulated cyclic displacement normalised by pile diameter for unfailed tests a) DP1-CY1 b) DP4-CY1 c) DP5-CY1 d) DP7-CY1 and e) retest DP4-CY2

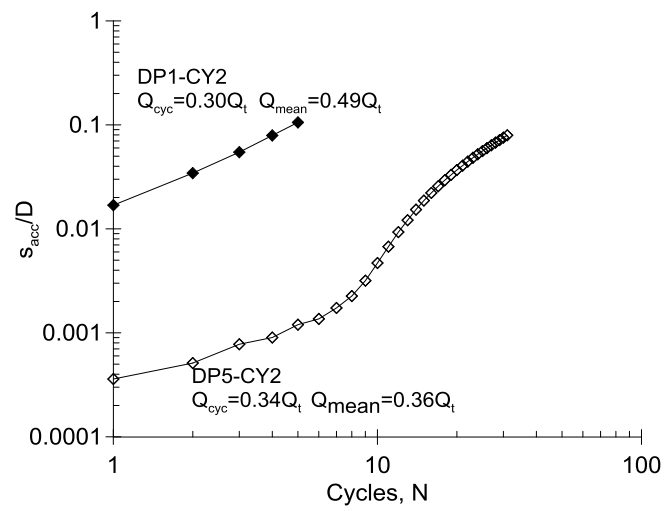


Figure 15 Permanent accumulated cyclic displacement normalised by pile diameter for failed tests

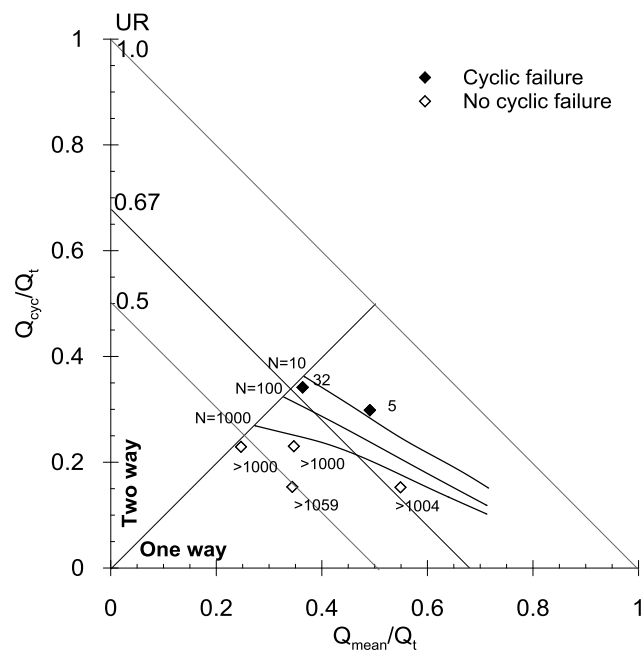


Figure 16 Cyclic loading interaction diagram with number of cycles either to failure or to the end of the test if unfailed

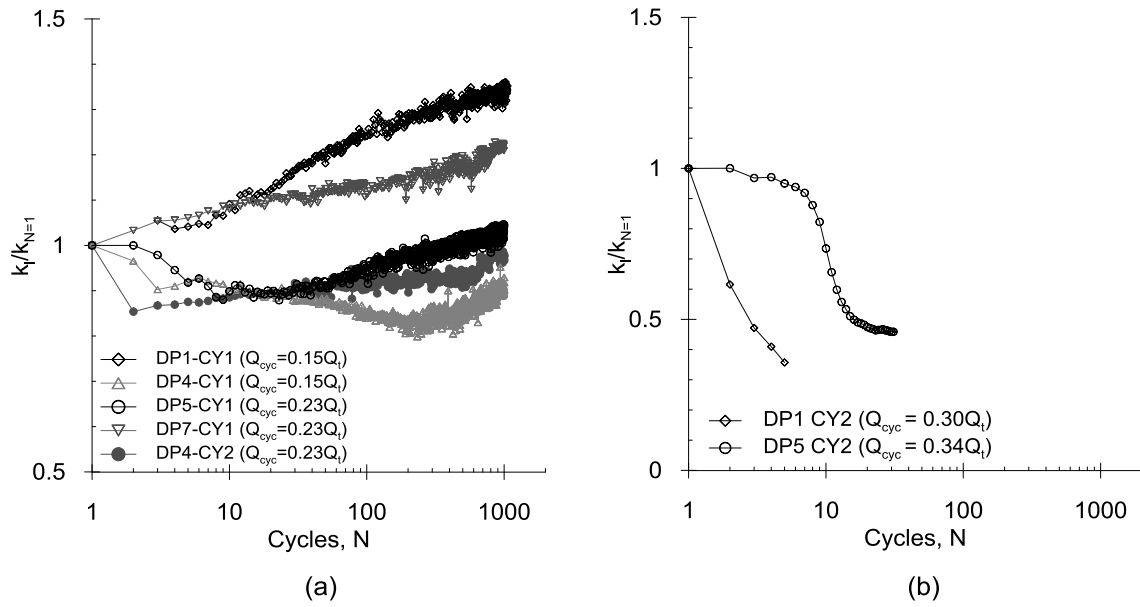


Figure 17 Global axial loading stiffness for tests for a) unfailed tests f b) failed tests

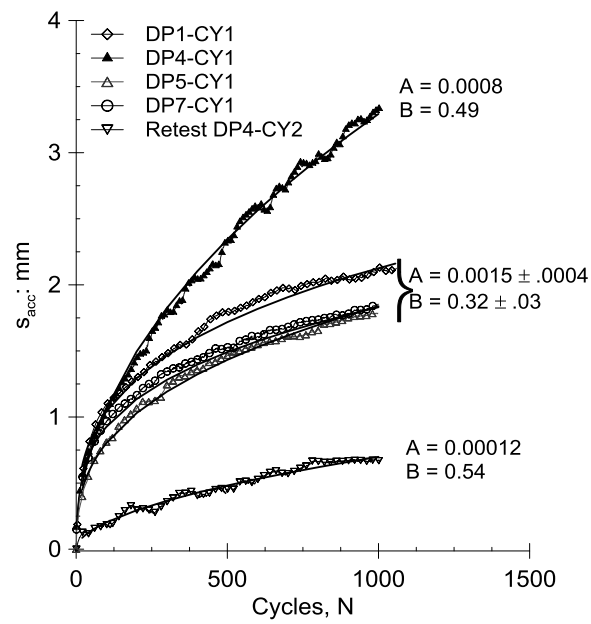


Figure 18 Permanent displacement accumulation with cycles for metastable/unstable tests on natural scale with power law fits and parameters shown

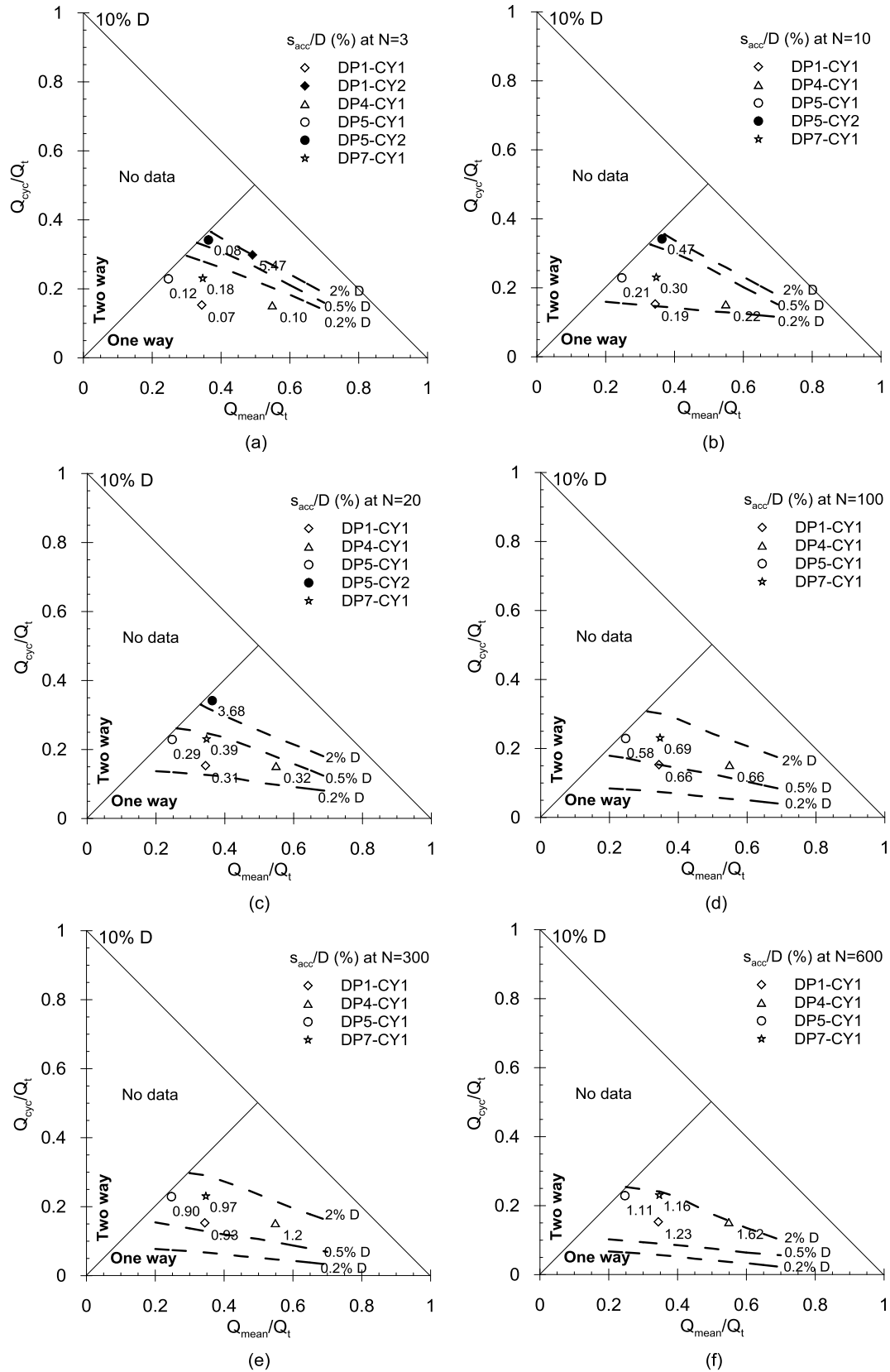


Figure 19 Cyclic interaction charts showing accumulated displacements (normalised by pile diameter) at a) N=3 b) N=10 c) N=20 d) N=100 e) N=300 and f) N=60

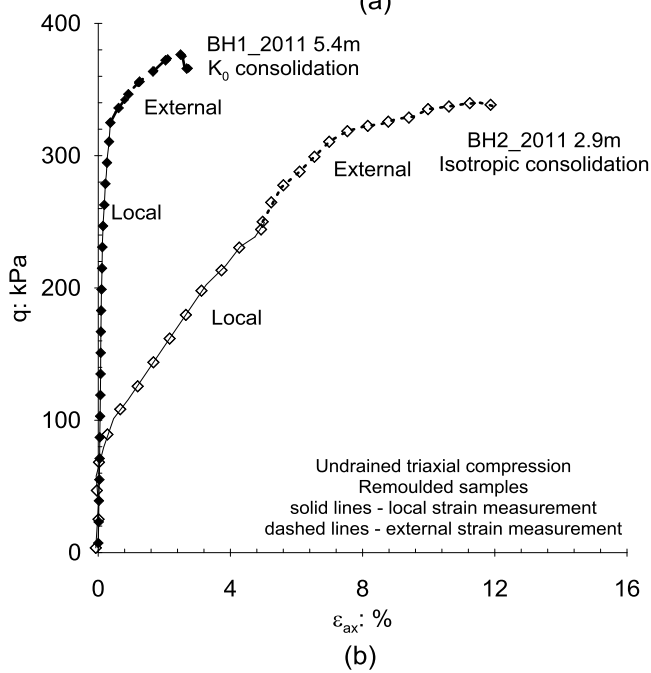
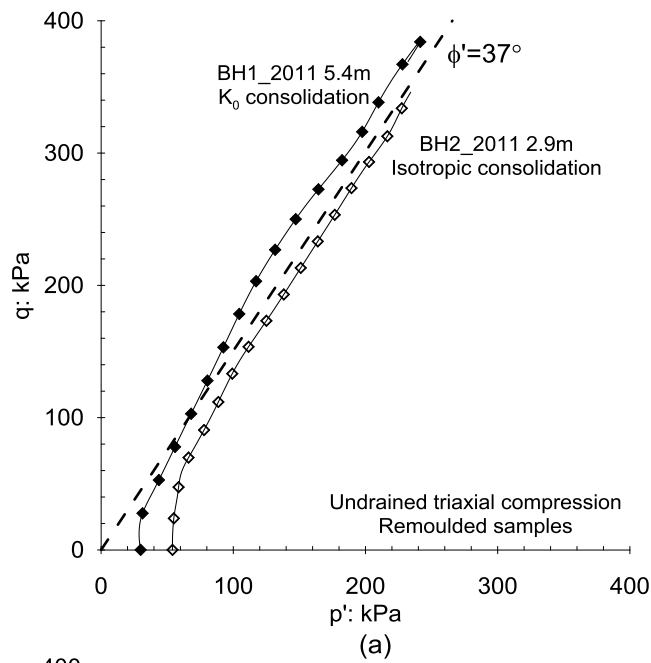


Figure 20 Undrained triaxial tests on remoulded samples a) stress paths in q - p' space b) q - ϵ_{ax}

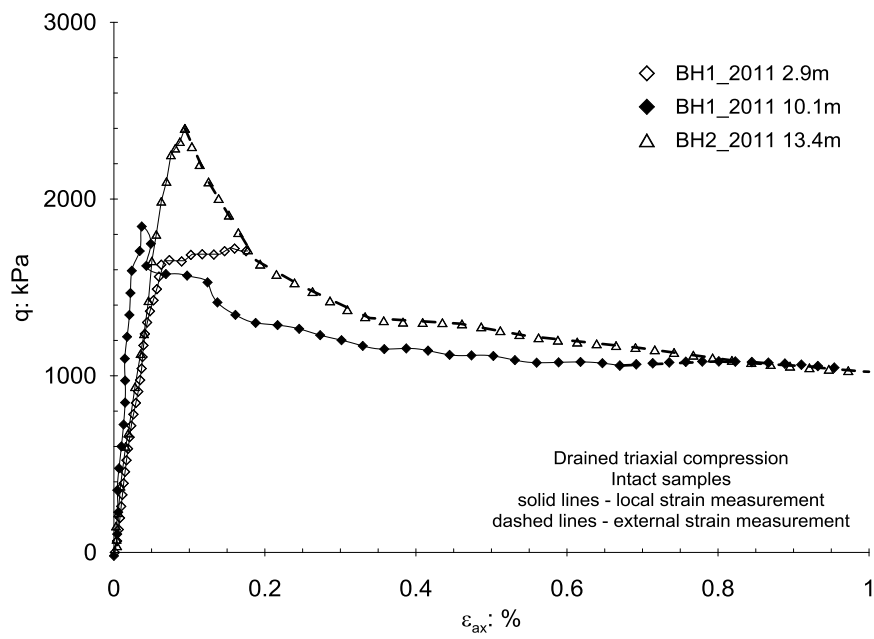


Figure 21 Drained triaxial tests on intact samples

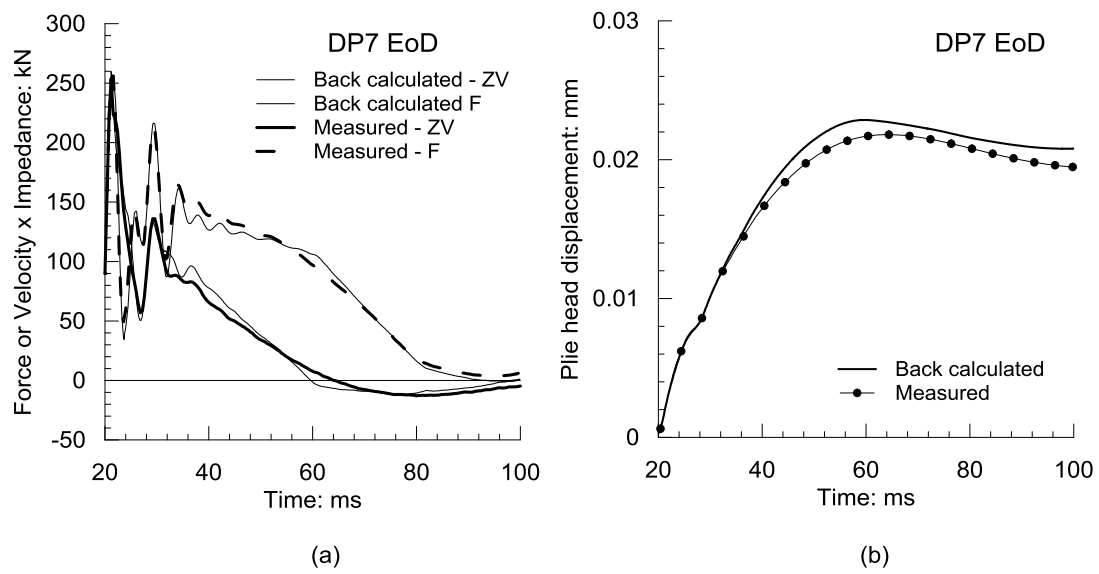


Figure 22 Signal matching results for pile DP7 a) force and velocity times impedance b) pile head displacement